ADVANCES IN THE DEVELOPMENT OF THE ESS-BILBAO PROTON INJECTOR

Z. Izaola,* I. Bustinduy, J. Corres, D. de Cos, C. de la Cruz, G. Harper, R. Miracoli, J. L. Muñoz, I. Rueda, A. Vizcaino and A. Zugazaga, ESS-Bilbao, Spain

Abstract

We present the last advances in the operation and construction of the ESS-Bilbao 3 MeV proton beam injector. The proton ECR source allows to change the distance between the plasma chamber and the first extraction electrode, acceleration gap. The beam has been characterised at different acceleration gaps by current transformers, wire scanners and photographs of 2d profiles. In addition, we present the status of the construction of the RFQ; which is at its beginning.

INTRODUCTION

ESS-Bilbao aims to develop an accelerator components for ESS.One of the main contribution is the Medium Energy Beam Transport (MEBT). If project schedule allows we plan to test the MEBT with a proton beam. To achieve this goal, we are building an injector composed of a proton Ion Source (ISHP) [1], Low Energy Beam Transport (LEBT) [2] and a Radio-Frequency Quadrupole (RFQ) [3].

The injector is expected to produce a proton beam with an energy of 45 keV and high intensity with a rms emittance around 0.25 π mm mrad in order to fulfil the requirements of the RFQ. One innovative feature of ISHP is the possibility to vary the gap between the plasma chamber and the extraction electrodes; the so called acceleration gap.

This paper, firstly, discuss the general layout of the LEBT. Secondly, it shows the result of various measurement campaign aiming to optimise and understand the beam. Finally, it discuss briefly the design of the RFQ and the current status of its construction.

* zunbeltz.izaola@essbilbao.org

THE LOW ENERGY BEAM TRANSPORT

The Bilbao Accelerator LEBT (Figure 1) is composed of two solenoids placed at fixed positions, producing tunable magnetic fields. The solenoids have a smaller internal radius (involving more turns) at their ends than in their centres [4]. This way, the magnetic field profile along the axis is flatter than the one achieved with an uniformly shaped solenoid; which would present a typical bell-shaped magnetic field profile. Besides, the variable radius approach creates a magnetic field that remains confined within the solenoid limits, avoiding perturbations on any nearby elements (e.g. other solenoids and the vacuum pump).

In order to save beam-line space, each solenoid includes a set of two crossed (x/y) dipoles of the $\cos\theta$ type. The dipoles are capable of steering the beam to correct for misalignment of the beam line components, reaching a deflection up to $\pm 4°$ of the protons. The presence of the dipoles limits the aperture to 100 mm [2].

Although the complete LEBT is equipped with three diagnostic boxes; one before the first solenoid, one between solenoids and one after the second solenoid; at this first stage we use only one solenoid and two boxes (Figure 2). The first box is equipped with an AC Current Transformer (ACCT1), a double-wire Wire Scanner (WS1) and a retractile beam collimator (BC) with a 5 mm radius hole to create a pencil beam. The second box contains a second ACCT2, a second WS (WS2), a quartz window for fluorescence measurements and a retractile beam shutter that protects the quartz. The two wires of the WS are at 45° from the horizontal and vertical directions. A Princeton Instrument CCD camera

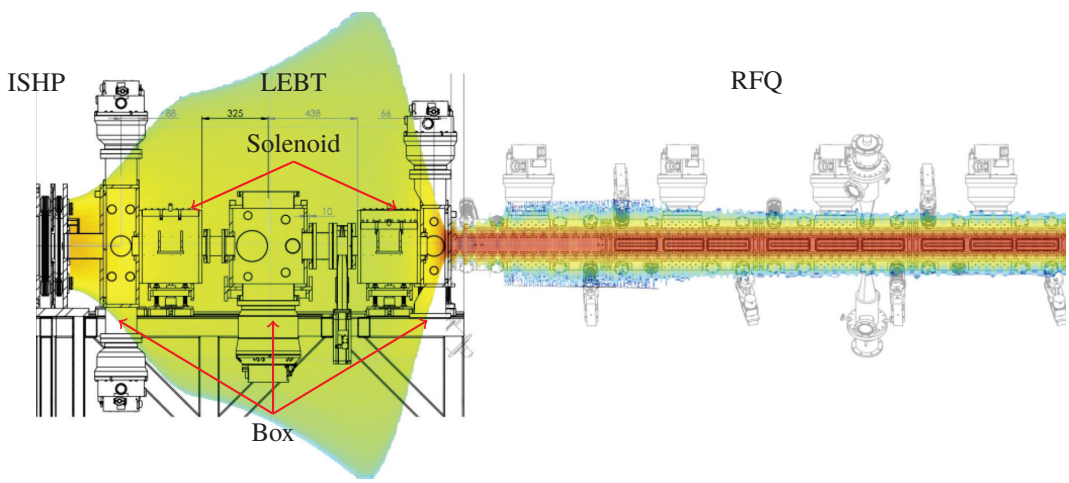

Figure 1: Schematic layout of the ESS-Bilbao injector from the H^+ Ion Source (left), through the LEBT (middle), to the RFQ (right). The coloured shadow represents the beam beam density along the injector.

ISBN 978-3-95450-178-6

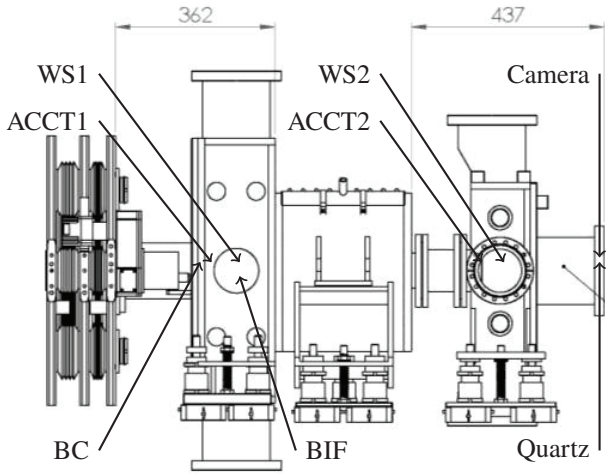

Figure 2: LEBT setup for the first stage of the beam commissioning.

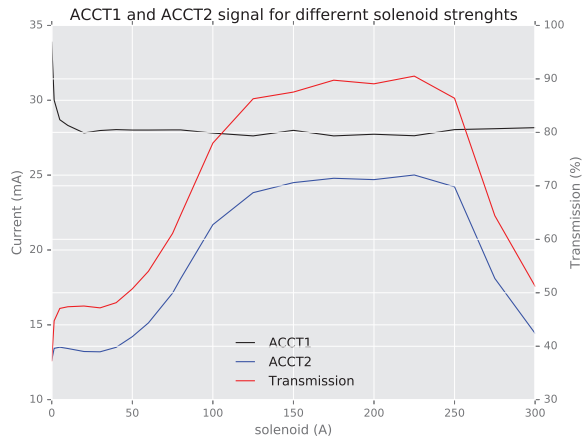

Figure 4: Beam current, before (ACCT1) and after (ACCT2) the solenoid, and transmission for different solenoid strengths.

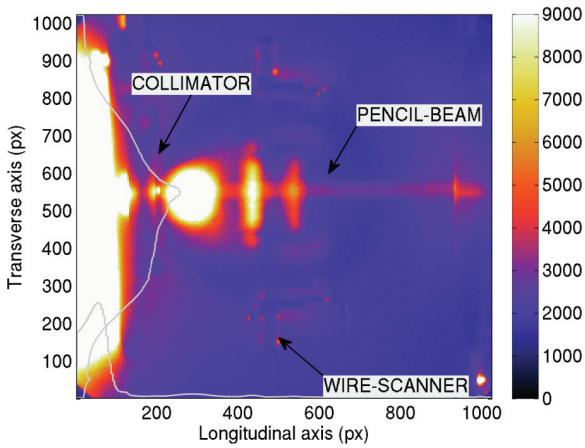

Figure 3: Image produced by the fluorescence induced by the collimated beam on the residual gas in the first diagnostics vessel of LEBT.

complements the quartz window in the exit port of the diagnostic box, for 2D profile photographs and pepper-pot measurements [5]. We used the camera also to record the Beam Induced Fluorescence (BIF) by mounting it in the side port of the first box (see Figure 3).

UNDERSTANDING THE BEAM

Our first goal was to find the acceleration gap with the highest transmission along the LEBT. Then, we studied 2D profiles of the beam; and this work lead to the investigation of different ion species in the beam.

Beam Current and Gap Optimisation

First we measured the effect of the solenoid strength in the transmitted beam current. The measurement was done with a 11 mm gap. Figure 4 shows that above 10 A on the solenoid power supply,[1] the beam current in the ACCT1 is stable. The elimination of the back-scattered electrons by the solenoid's fringe field may be the reason of beam current reduction at 10 A. Therefore, we will use 10 A as the baseline solenoid configuration to compare with. The transmitted beam current start increasing at ~150 A; reaching a plateau between 150 A to 180 A and reducing later, due to over-focusing of the beam.

The next step in the way of understanding the beam was to optimise the extraction gap. We measure 95 different beam profiles with extraction gaps between 8 mm and 14 mm, and solenoid currents between 10 A and 300 A.

Different ways were employed to characterise the beam concentration in the rms area. A graphic one was to study the collimated beam in the first diagnostic box, and measuring the Gaussian height and widths (Figure 3). The results agree with the ones presented in Figure 5. This Figure shows the transmission of the LEBT without the solenoid focalisation effect (10 A to avoid measuring secondary electrons). Although the higher current is achieved for the smallest gaps as foreseen, the best transmission is somewhere between 9 mm and 10 mm. When solenoid is energised transmission values are improved up-to 80 % for all different gaps.

The WS1 (see Figure 6 show that the beam profiles is far from being Gaussian. The fringe fields of the solenoid at 300 A reduce the background measured by the WS1. Even thought, the central part of the beam shows a quite flat top with two small peaks. The effect of the fringe fields is more pronounced for the horizontal signal than the vertical; causing a less symmetric beam. At shorter gaps the beam seems a bit more focused and therefore, less sensitive to the small effects of the fringe fields.

In summary; we get the highest beam intensity for the shortest gap, where the maximum transmission is for the

[1] The relation between power supply current and magnetic field is $B(\mathrm{T}) = 0.0013 \times I(\mathrm{A})$. So 10 A corresponds to 0.013 T, 100 A to 0.13 T, 150 A to 0.2 T, 180 A to 0.25 T and 300 A to 0.4 T.

ISBN 978-3-95450-178-6

Figure 5: Transmission with the solenoid at 10 A for different acceleration gaps. Measurement at equal gaps have the same colour and some data have been displaced from the corresponding gap in the abscissa direction for a better display.

Figure 6: Beam profile measured by WS1 at 9.5 mm gap.

9 mm gap. With this data in mind, we select the region around 8.5 mm and 9.5 mm as the optimum acceleration gap from the point of view of beam intensity. Most importantly, the effect of the gap in the beam profile is smaller that we expected initially.

Beam 2D Distribution

The measured beam profiles incite us to make photographs of the beam to understand better the shape of the beam. The beam impacted a quartz windows whose upstream face is coated with a 50 Å aluminium layer. The luminescence produced in the quartz was recorded by a CCD camera. The aluminium layer prevented the direct light of the ion source to reach the camera. All the images where done with the solenoid at 10 A, without focusing the beam.

We found repeatedly, different distributions of the beam intensity on the quartz screen. Figures 7 and 8 show only two

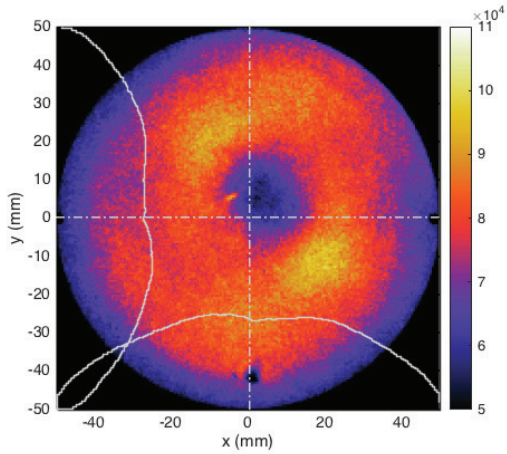

Figure 7: Photo of extracted beam for configuration family5.

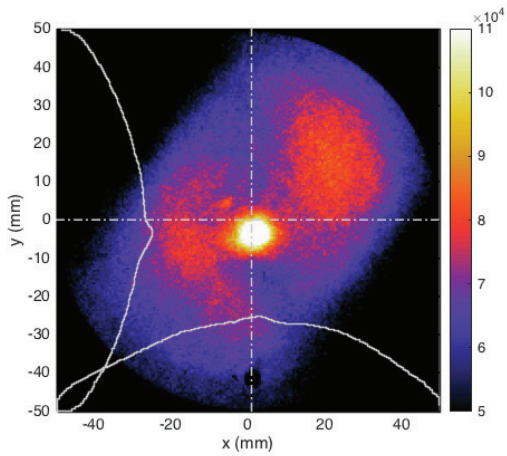

Figure 8: Photo of extracted beam for configuration family7.

examples of different identified *beam shapes.* We classified all recorded shapes in 5 *families.*

This families are reproducible with certain values of the confinement-magnetic-field coils and the input H_2 flow (see Table 1) of the ion source.

Previous research with a similar ion source at ESS-Bilbao [6], found plasma distributions that resembled the beam distribution shown in Figures 7 and 8. Different relative compositions of H^+, H_2^+ and H_3^+ were found. It shall be stressed that the imaged reported here are of *extracted beam,*

Table 1: Plasma Parameters of the Different "families."

Family	3	4	5	7	10
H_2 (%) flow	42	42	42	23	44
Coil#1 (A)	2	2	2	2	2
Coil#2 (A)	5.1	2	3.5	3.9	7.1
Coil#3 (A)	10	10	10	10	7.5
Coil#4 (A)	3.5	5.8	4.5	3.5	4.4

ISBN 978-3-95450-178-6

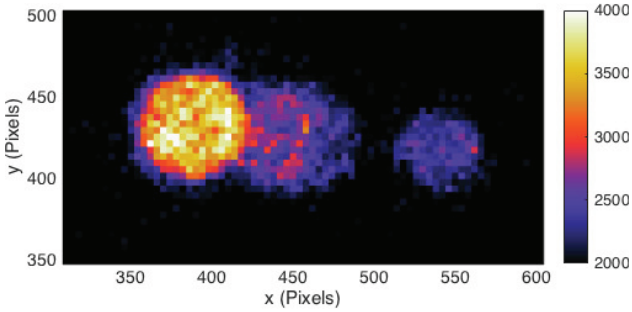

Figure 9: 2D beam profile with second steerer at 12 V for family5.

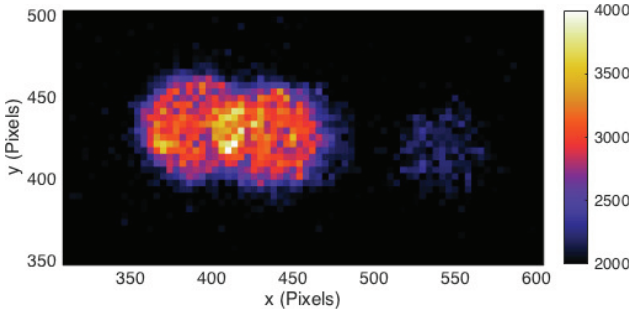

Figure 10: 2D beam profile with second steerer at 12 V for family7.

rather that of the plasma itself as in the cited paper, and were measured at 734 mm distance from the plasma meniscus.

Ion Specimens Present in the Beam

With this in mind, we intended to correlate each family with the specimen concentration. Although WS2 profiles were also used to identify different specimen peaks [7], we set up the following experiment: 2D beam profiles of the collimated beam where recorded with the camera for different values of the steering magnet; while the solenoid was off. Figures 9 and 10 show how the steerer splits the collimated beam into different specimens for the family5 and family7 configurations

The photograph showed three spots separated horizontally. Profiles by integration of the vertical axis are shown for family5 is in Figure 11 and for family7 in Figure 12. The profiles of the other families are very similar to the profile of family5, and, therefore, only the results of this family are presented. Fitting the data to 3 Gaussian peaks and using a conversion factor of 0.19 mm px^{-1} provided by a calibration image, the distance between peaks can be calculated (see Table 2).

To test the initial hypothesis that the 3 peaks represent H^+, H_2^+ and H_3^+, we performed two TraceWin simulations. The initial beam has 0.5 π mm mrad emittance in both x and y planes. The energy is 45 keV and the current is 80 mA; 50 % of H^+ and 50 % of H_2^+ in the first simulation and 50 % of H^+ and 50 percent of H_3^+ on the second.[2] The aim of the

[2] At the time of the doing the simulations, it was not possible to use more than two particle specimen in TraceWin.

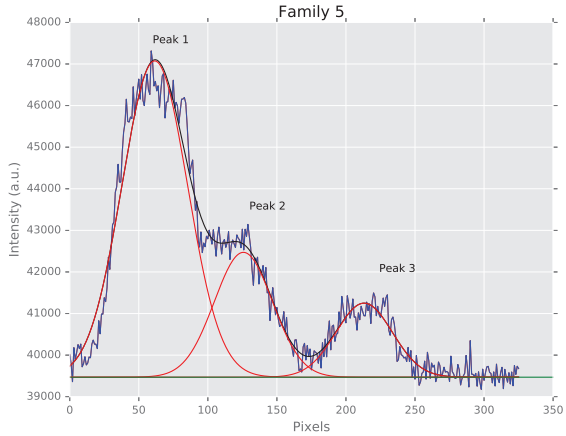

Figure 11: Horizontal profile with second steerer at 12 V for family5.

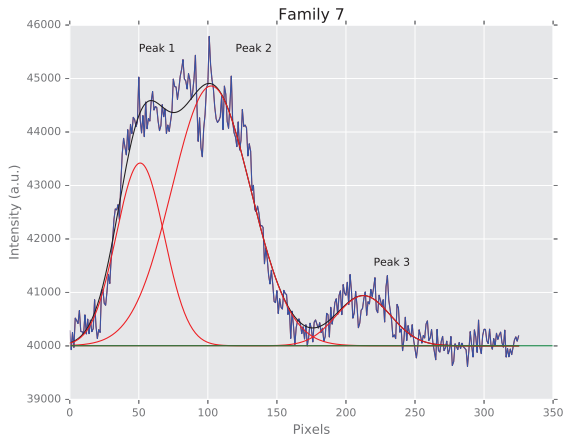

Figure 12: Horizontal profile with second steerer at 12 V for family7.

simulation is not to match the height of the peaks but their relative position; therefore the exact current of each beam is not important. Furthermore, to obtain a good statistic after the hole in the beam collimator, a initial high current is needed. The space-charge compensation is 90 %. The distance between the exit of the steerer and the scintillator screen is 252 mm. In order to accurately represent the experimental setup, measured field maps [8] were used for both solenoid and steerer components. A 60 000 point grid was gathered for each magnetic component (B_x, B_y, B_z) and was latter superimposed in TraceWin.

The simulations show that the H^+ peak shifted from the centre 30.9 mm; the H_2^+ 21.4 mm and the H_3^+ 17.1 mm. Table 2 compare this results with the ones from the experiments. From these values, we can assign peak #1 to H^+ with great confidence. Peak #3 seems to be due to particles heavier than H_3^+ because they are not displaced so much. It is still unclear what is the nature of those particles; they may be heavier ions coming out the plasma (impurities). Peak #2 is

ISBN 978-3-95450-178-6

Table 2: Position (relative to the collimator centre) and composition for families 5 and 7; and simulated positions of peaks relative to beam pipe centre.

	Position [mm]			Composition (%)		
Peak	#1 H^+	#2 H_2^+	#3 H_3^+(?)	#1 H^+	#2 H_2^+	#3 H_3^+(?)
Family5	30.2	18.1	1.4	64	23	13
Family7	32.1	22.4	1.3	24	67	9
Simul.	30.9	21.4	17.1			

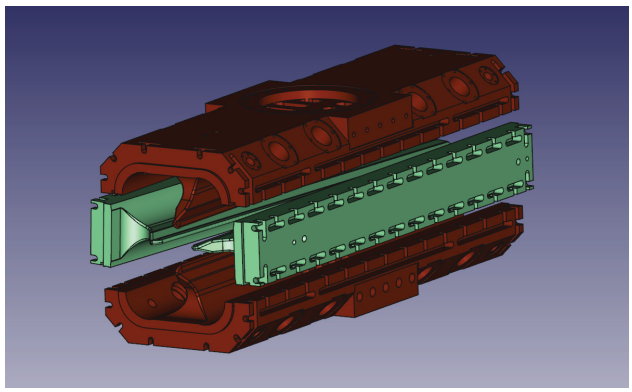

Figure 13: CAD image of the RFQ's first segments.

between the peaks of H_2^+ and H_3^+, so it maybe be due to the H_2^+ and other ion with a similar q/m ratio.

Integrating the fitted Gaussian allows to calculate the relative composition of the beam. Table 2 shows that the composition of H^+ and H_2^+ is very different in families 5 and 7. Furthermore, in the best of the cases, only 2/3 of the beam current is due to H^+ ions.

Measurements with the WS2 in the same conditions showed qualitatively similar results. Because the steerers move the peaks in the horizontal direction (as seen in the photographs), and the WS measures on a 45° angle, the peaks are seen on both wires of the WS.

RADIO-FREQUENCY QUADRUPOLE

The ESS-Bilbao Radio-Frequency Quadrupole (RFQ) [3] is designed to accelerate the proton beam from 45 keV to 3 MeV. It is a pulsed machine (duty cycle 4 %), operating at a frequency of 352.21 MHz. Design has finished and public procurement has started on June 2015.

The RFQ has total length of 3.12 m (3.86 λ) and will be assembled from four segments (see Figure 13) using Polymeric vacuum gaskets. The modulation of ESS-Bilbao RFQ is the result of an optimisation process based on a 2-term expansion (with a uniform 85 kV inter-vane voltage) using a modified version of RFQSIM code. The modulation has been verified using different codes: Toutatis, GPT+COMSOL and PARMTEQ/RFQGen. The overall transmission is between 87 % and 94 %.

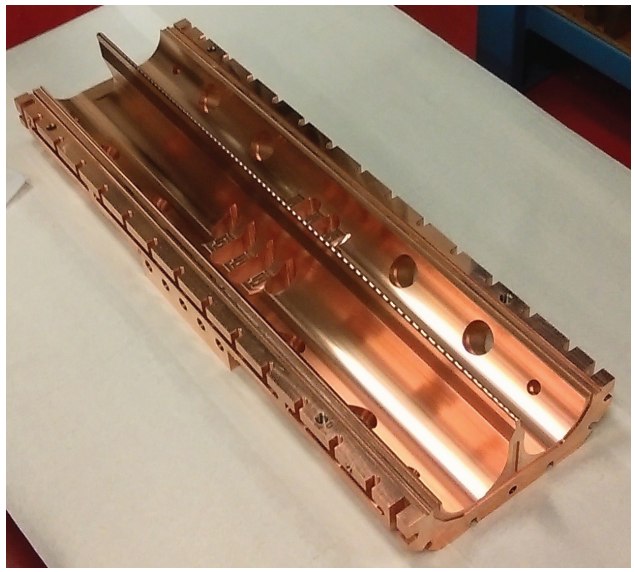

Figure 14: Major vane of the first section after fine machining.

The first segment of the RFQ is currently under fabrication (Figure 14). The first major vane is already finished and metrology is expected for June. When the four vanes are machined, they will be assembled and measured, and a final machining of the vacuum gaskets in the end faces will be done. This is expected for the last quarter of 2016. Mechanical and RF tests will be carried out with the first segment of the RFQ before the machining of the remaining three segments can start. Final assembly and tests with the whole RFQ are planned for late 2017.

CONCLUSIONS

The effect of the plasma parameters on the extracted beam profiles (Figures 10 and 9) is greater than we expected, if compared to the effect of the acceleration gap in these profile (Figure 6). Different ion source configurations show unlike profiles, not only in the plasma but also in the extracted beam, that are far from being "ideal Gaussian beam."

FUTURE WORK

The most important step in the following months is to measure the emittance of the beam. Other measurements include to search plasma parameters with a higher H^+ concentration. After this first characterisation of the beam is done, the whole LEBT will be installed. The final goal of the LEBT commissioning is to create a "map" of the emittance of the beam at the RFQ position for different configurations of the LEBT solenoids and steerers.

ACKNOWLEDGEMENT

The authors will like to acknowledge the work of all the staff at ESS-Bilbao in the design, building and running of the different parts of the injector.

ISBN 978-3-95450-178-6

REFERENCES

[1] J. Feuchtwanger et al. "Status of the Ion Sources at ESS-Bilbao." In: *Proceedings of IPAC2012*. TUPPC030. New Orleans, Louisiana, (USA), 2012.

[2] I Bustinduy et al. "First LEBT simulations for the Bilbao accelerator ion source test stand." In: *Procedings of HB2010*. 2010.

[3] Ibon Bustinduy and J. L. Muñoz, eds. *Technical Design Report: ESS-Bilbao RFQ*. 2nd ed. 2015. ESS-Bilbao Consortium Report Series ESSB-Rep-2015-010. Feb. 12, 2015. 330 pp. ISBN: 978-84-616-5445-1.

[4] J. Pozimsk et al. "Particle Dynamics Calculations and Emittance Measurements at the FETS." In: *Proceedings of LINAC 2006*. TUP066. Knoxville, Tennessee (USA), 2006.

[5] S. Jolly et al. "Data Acquisition and Error Analysis for Pepperpot Emittance Measurements." In: *DIPAC09 Conference Proceedings*. 2000.

[6] O. D. Cortázar et al. "Correlations between density distributions, optical spectra, and ion species in a hydrogen plasma (invited)." In: *Review of Scientific Instruments* 87.2 (2016). DOI: http://dx.doi.org/10.1063/1.4931720. http://scitation.aip.org/content/aip/journal/rsi/87/2/10.1063/1.4931720

[7] Zunbeltz Izaola et al. *Spectroscopy study of the beam for different plasma parameters*. Tech. rep. LEBT-BP-M006-FV. ESS-Bilbao, 2015.

[8] I. Bustinduy et al. *LEBT Solenoid Review*. LEBT-LD-IR15-V1-SOL-IBustinduy. ESS-Bilbao.

ISBN 978-3-95450-178-6